

基于液体对太赫兹脉冲进行高灵敏探测

王国阳¹, 张明浩¹, 肖文¹, 张存林¹, 王伟民², 张亮亮^{1*}¹首都师范大学物理系太赫兹光电子学教育部重点实验室, 北京 100048;²中国人民大学物理系, 北京 100872

摘要 由于液体(尤其是液态水)对太赫兹波的强吸收,以液体为介质的太赫兹波产生和探测长期以来被认为是无法实现的。本文综述了基于液体的太赫兹相干探测方法,此方法能在更低的探测激光能量下实现更高的探测灵敏度,可以解决目前基于固体和空气的探测方法遇到的探测频带受限、探测激光能量过高的问题。该探测方法的工作机理被归结为飞秒激光与太赫兹波在液体等离子体中的四波混频过程,因此太赫兹波与探测激光、产生的二次谐波间的场强、偏振具有简单的依赖关系,这使得此方法具有良好的稳定性,并可用于太赫兹波偏振敏感光谱的检测。液态水对太赫兹波的强吸收限制了检测灵敏度的进一步提高,可以利用其他液体或溶液替代纯水来降低太赫兹波的吸收,提高探测灵敏度,这对于该探测方法的进一步推广具有重要意义。

关键词 非线性光学; 太赫兹波; 相干探测; 液体等离子体; 四波混频

中图分类号 O437 文献标志码 A

DOI: 10.3788/CJL230725

1 引言

太赫兹波 (THz) 是指频率在 0.1~10 THz 的电磁波^[1-5], 介于微波与红外频段之间^[6-7]。随着飞秒激光器的发展, 太赫兹波在成像技术^[8-13]、通信技术^[14]、医疗卫生^[15-16]、生物化学技术^[17]、无损检测^[18]、安检技术等领域的的应用越来越广泛。目前产生的太赫兹波的能量较低, 高灵敏度和大带宽的探测技术是亟待解决的问题。在太赫兹波相干探测领域应用最广的是基于固体介质的光电导采样技术和电光采样技术, 然而, 受介质载流子非瞬时响应、声子吸收、Reststrahlen 频带等因素的影响, 其探测带宽难以覆盖整个太赫兹波段。气体介质不受这些因素的影响, 可以通过空气偏置相干检测和光场偏置相干检测的方法实现足够宽频太赫兹波的相干探测。但是, 为了实现足够高的探测灵敏度, 需要用探测飞秒激光束将空气电离成等离子体, 而空气的激发阈值较高, 通常需要激光束的能量为几百微焦。固体和气体已被证明是探测太赫兹波^[19-23]的介质, 而液体是否能用于太赫兹波的相干探测一直是太赫兹领域研究人员感兴趣的重要课题。有研究证实液体能用于太赫兹波的产生^[24-25], 而且产生的太赫兹波的强度比空气产生的太赫兹波提高了 1.8 倍。与气体相比, 液体具有较大的分子密度和非线性系数, 这使得液体等离子体具有较大的自由电子浓度和较低的电离阈值^[26-27]。与固体相比, 液体的损伤阈值更高, 而且可以自修复。

本文主要综述了基于纯水、盐溶液和乙醇的宽带太赫兹脉冲的相干探测。由于液体的三阶非线性系数比空气大, 在相同能量的探测激光下, 液体等离子体产生的二次谐波成分大约是空气的 100 倍。在相同的条件下, 与空气相比, 液体探测所需的激光能量更低, 探测带宽更大, 灵敏度更高。盐溶液和乙醇的三阶非线性系数比纯水更高, 可以进一步提高探测灵敏度和信噪比。基于液体的太赫兹波相干探测方案拓宽了太赫兹波探测器的种类, 为揭示液体环境中的分子相互作用机制提供了可能性。

2 液体探测太赫兹脉冲的基本原理

液体探测太赫兹波的系统如图 1 所示。用一对线栅偏振片 (TPs) 控制太赫兹的电场强度, 离轴抛物面镜 (PM) 将太赫兹波聚焦到水等离子体上。能量大于 2 μJ 的 800 nm 探测激光聚焦激发水膜形成水等离子体; 50 μm 厚的偏硼酸钡 (BBO) 晶体放置在探测光路上, 以产生受控二次谐波 (CSH)。CSH 与太赫兹波诱导的二次谐波 (TISH) 共同透过 400 nm 滤波片后被光电倍增管 (PMT) 探测。

根据四波混频机制, TISH 的电场强度的大小 $E_{\text{TISH}} \propto \chi^{(3)} E_{\omega}^2 E_{\text{THz}}$, 实验中测得 TISH 和 CSH 相干后的能量为

$$I_{2\omega} \propto |E_{\text{TISH}} + E_{\text{CSH}}|^2 \propto |\chi^{(3)} E_{\omega}^2 E_{\text{THz}}|^2 + |E_{\text{CSH}}|^2 + 2\text{Re}[\chi^{(3)} E_{\omega}^2 E_{\text{THz}} E_{\text{CSH}}], \quad (1)$$

收稿日期: 2023-04-17; 修回日期: 2023-05-21; 录用日期: 2023-06-15; 网络首发日期: 2023-06-26

基金项目: 国家自然科学基金(12074272, 61905271)、中国国防科技创新特区项目(20-163-02-ZT-008-009-01)

通信作者: *liangliang_zhang@cnu.edu.cn

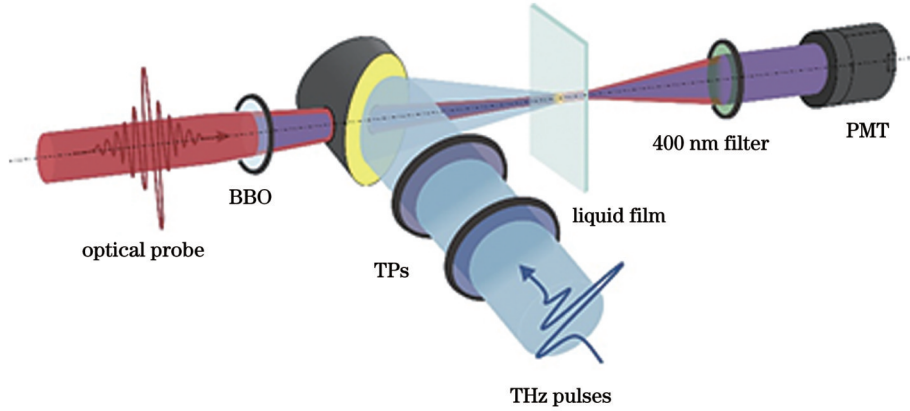


图 1 液态水中 TISH 测量系统示意图^[28](BBO: 偏硼酸钡晶体; TPs: 太赫兹波偏振器; PMT: 光电信增管)

Fig. 1 Schematic of TISH measurement system in liquid water^[28] (BBO: barium metaborate crystal; TPs: terahertz polarizer; PMT: photomultiplier tube)

式中: $\chi^{(3)}$ 表示液体的三阶非线性系数; E_ω 表示基频光的电场强度的大小; E_{THz} 表示太赫兹电场强度的大小; E_{CSH} 为受控二次谐波的电场强度的大小。

考虑到基频光和倍频光的脉宽约为 50 fs, 远小于探测器的积分时间, 因此实验中观察到的信号为

$$S_{2\omega}(t_{\text{THz}}) \propto \int_{-\infty}^{+\infty} |\chi^{(3)} E_\omega^2(t) E_{\text{THz}}(t + t_{\text{THz}})|^2 dt + \int_{-\infty}^{+\infty} E_{\text{CSH}}(t) E_{\text{CSH}}^*(t) dt + 2\text{Re} \int_{-\infty}^{+\infty} \chi^{(3)} E_\omega^2(t) E_{\text{CSH}}^*(t) E_{\text{THz}}(t + t_{\text{THz}}) dt. \quad (2)$$

式(2)中的第二项为直流噪声, 可以通过斩波器配合锁相放大器消除。第一项对应非相干探测, 第三项对应相干探测。由于本实验中 BBO 倍频晶体提供的 CSH 单脉冲能量在 $10^{-5} \mu\text{J}$ 量级, 被积函数 $|\chi^{(3)} E_\omega^2 E_{\text{THz}}| \ll |\chi^{(3)} E_\omega^2 E_{\text{CSH}} E_{\text{THz}}|$, 此时相干探测适用。对于相干探测项,

$$E_\omega^2(t) E_{\text{CSH}}^*(t) = |E_\omega^2(t)| |E_{\text{CSH}}^*(t)| \exp(i\phi), \quad (3)$$

因此测量的信号可以近似表示为

$$S_{2\omega}^{\text{coherent}}(t_{\text{THz}}) \propto \cos \phi \int_{-\infty}^{+\infty} I_\omega(t) \sqrt{I_{\text{CSH}}(t)} \text{Re}[E_{\text{THz}}(t + t_{\text{THz}})] dt + \sin \phi \int_{-\infty}^{+\infty} I_\omega(t) \sqrt{I_{\text{CSH}}(t)} \text{Im}[E_{\text{THz}}(t + t_{\text{THz}})] dt, \quad (4)$$

式中: ϕ 为基频光和倍频光之间的相位差。

近似将太赫兹脉冲视为单色波, 即 $E_{\text{THz}}(t) \propto \cos(\omega_{\text{THz}}t) + i \sin(\omega_{\text{THz}}t)$, 其中

$$\text{Im}[E_{\text{THz}}(t)] = \text{Re}[E_{\text{THz}}(t + \pi/2)], \quad (5)$$

那么实验测量值可以记为

$$S_{2\omega}^{\text{coherent}}(t_{\text{THz}}) \propto |I_\omega \sqrt{I_{\text{CSH}}}| [E_{\text{THz}}(\omega_{\text{THz}}t_{\text{THz}})] \cos \phi + |I_\omega \sqrt{I_{\text{CSH}}}| [E_{\text{THz}}(\omega_{\text{THz}}t_{\text{THz}} + \pi/2)] \sin \phi. \quad (6)$$

根据式(6), 可以基于液态水等离子体实现对太赫兹脉冲的相干探测。当太赫兹脉冲被阻断时, 可测

量空气和水等离子体中超连续辐射的本地二次谐波。图 2(a) 和图 2(b) 分别表示空气和水等离子体中的二

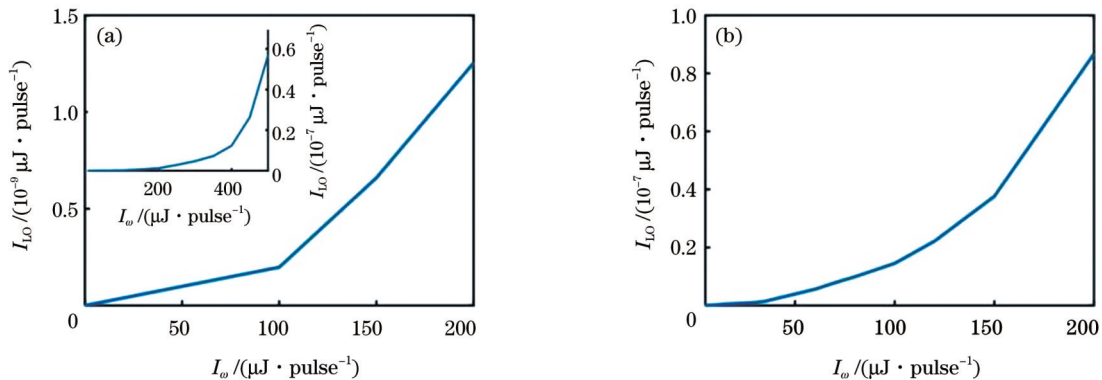


图 2 空气和水等离子体中超连续辐射的二次谐波强度与探测光能量的关系^[28]。(a) 空气等离子体; (b) 水等离子体

Fig. 2 Intensity of SH in the supercontinuum radiation of air and water plasmas versus probe energy^[28]. (a) Air plasma; (b) water plasma

次谐波强度^[28]。在该实验中,当探测激光能量超过 200 μJ 时,重力驱动的水膜破裂。当激光能量超过水膜的损伤阈值时,在两个相邻激光脉冲(1 ms)的时间间隔内,水膜很难恢复。图 2(a)和图 2(b)是仅在单脉冲能量小于 200 μJ 时测量得到的。图 2(a)中的插图显示了在空气等离子体中由高能脉冲激发的测量结果。在水等离子体中产生的二次谐波的强度大约是在空气中产生的 100 倍,这是由于与空气相比液体的非线性系数较大。

太赫兹脉冲入射水膜后,等离子体中的二次谐波大大增强,通过延时扫描可得到 TISH 的时域波形。图 3 为水等离子体中 TISH 的时域波形^[28]。由四波混频模型拟合结果可以看出,TISH 强度与太赫兹波的强度成正相关。然而,由于相位信息完全丢失,只能得到 TISH 强度与太赫兹脉冲的振幅成平方关系。

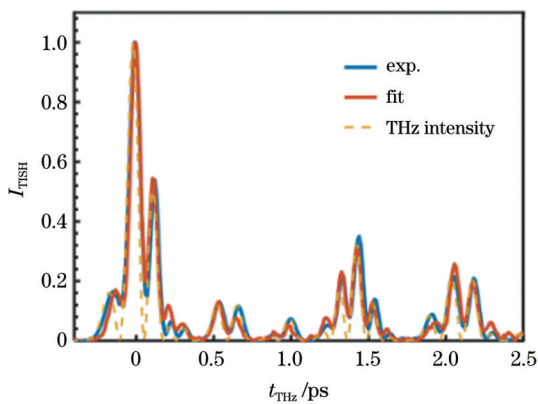


图 3 水等离子体中 TISH 的时域波形^[28],其中红线为基于四波混频原理的拟合结果,虚线为太赫兹波强度

Fig. 3 Time-domain waveform of TISH in water plasma^[28], where the red line is the fitting result based on the four-wave mixing mechanism, and the dashed line represents the intensity of terahertz wave

TISH 强度与太赫兹电场强度呈二次方关系,如图 4 所示,拟合结果与实验数据吻合较好。

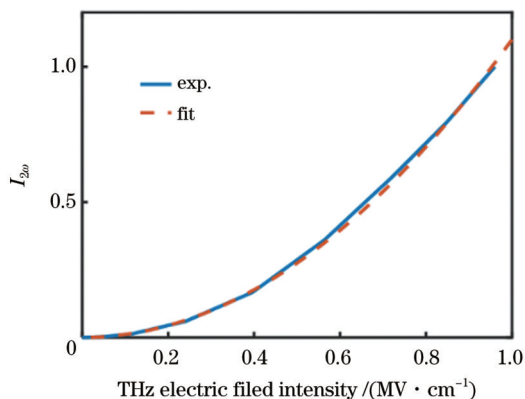


图 4 TISH 强度与太赫兹电场强度的依赖关系曲线^[28]

Fig. 4 Dependence of TISH intensity on terahertz electric field intensity^[28]

3 基于液态水的宽带太赫兹脉冲的相干探测

2022 年,谭勇等^[29]首次实现了基于液态水的宽带太赫兹脉冲的相干探测。他们通过将水等离子体中产生的 TISH 与 CSH 结合,得到了频率范围为 0.1~18 THz 的太赫兹波时域波形,并证明了其产生原理为四波混频。与空气探测相比,液态水所需的探测激光能量要低得多,只有几微焦,而探测灵敏度却高一个数量级。因此,液态水探测适用于缺乏高激光能量的场合,比如探测激光在光路中显著消耗并且需要传播较长距离才能与太赫兹电场混合的场合。

实验原理图如图 5(a)所示^[29],当探测光能量在 2 μJ 以上时,将垂直方向的 800 nm 探测光与竖直偏振的太赫兹波共聚焦在厚度为 90 μm 的自由流动水膜上,形成水等离子体。然后,探测光通过一个 400 nm 的窄带滤波器,之后进入光电倍增管(PMT),PMT 测量水等离子体发射的 400 nm 二次谐波。当将 50 μm 厚的 BBO 晶体放置在 800 nm 探测光的路径上时,可以产生 CSH 光束,CSH 光与基光共线传播。当 CSH 光束垂直偏振并与 TISH 光束相干时,采集到的信号中出现了一个与太赫兹电场强度呈正相关的线性分量。这提供了一种同时测量太赫兹波振幅和相位的方法。为了证明这种液态水探测方案的可行性,测量了太赫兹脉冲的时域波形及其相应的频谱,如图 5(b)和图 5(c)所示。为了将测量结果与电光取样探测(EOS)结果进行比较,使用低通滤波器将太赫兹脉冲的带宽限制在 6 THz 以下,并将太赫兹电场强度控制在 0.3 MV/cm,以确保厚度为 100 μm 的磷化镓晶体能够进行有效探测。考虑到复响应函数,重建了太赫兹脉冲^[30-32]的波形和频谱,如图 5(b)和图 5(c)中的红色虚线所示。两种探测方法得到的太赫兹波形和波谱的测量结果吻合得较好,证明了基于液态水的相干探测的可靠性。

3.1 相位和偏振的依赖性

为了捕获测量信号对相对相位的完全依赖性,记录了太赫兹脉冲的时域波形,同时通过沿光路平移 BBO 晶体来控制探测光和 CSH 的相位差。图 6(a)~(d)给出了带宽分别为 2、3、6、18 THz 时测得的太赫兹脉冲波形随相位差的变化,其与图 6(e)~(h)所示的模拟结果一致^[28]。

为证明该方法对太赫兹波偏振的依赖性,测量了 TISH 能量对探测光与太赫兹电场之间相对偏振角的依赖性。实验中,探测光束固定为垂直偏振,旋转太赫兹波的偏振方向。在无 CSH 的情况下,TISH 能量与相对偏振角的关系如图 7(a)所示。图 7(b)是有 CSH 时测量信号对相对偏振角的依赖性^[29]。结果表明,该方案是偏振灵敏的相干探测,可以通过适当旋转探测光的偏振方向分别探测太赫兹电场的两个正交分量。

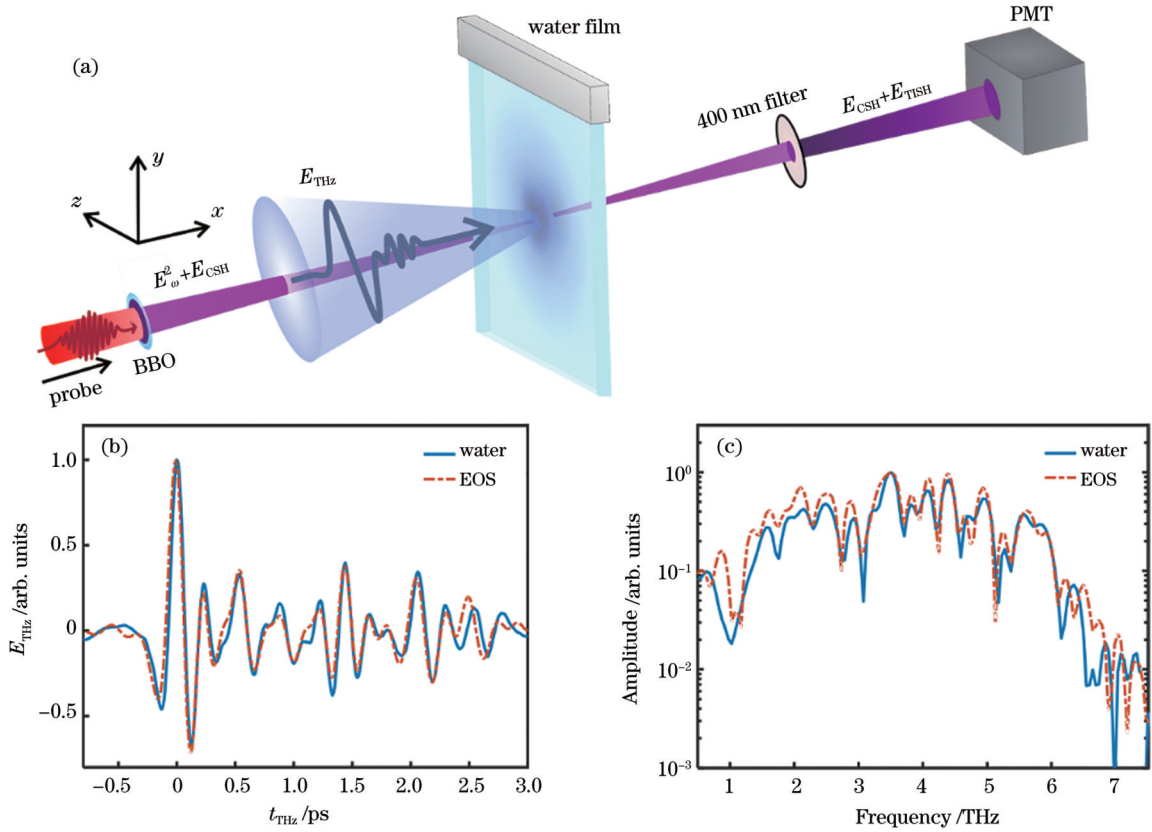


图 5 基于液态水的太赫兹波相干探测实验装置示意图以及测得的太赫兹波形及相应的频谱^[29]。(a)实验装置示意图；(b)(c)测得的太赫兹波形及相应的频谱

Fig. 5 Schematic of the water-based terahertz wave coherence detection experimental setup and measured terahertz waveforms and the corresponding frequency spectra^[29]. (a) Schematic of experimental setup; (b) (c) measured terahertz waveforms and the corresponding frequency spectra

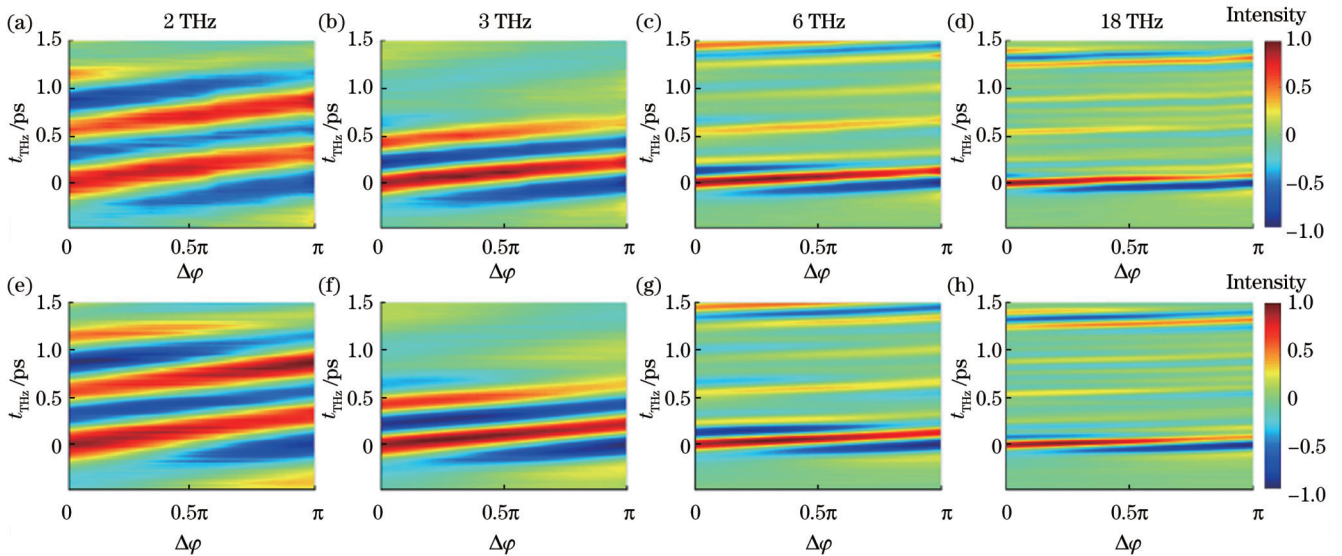


图 6 带宽分别为 2、3、6、18 THz 时，太赫兹信号随时间延迟和相位差的变化^[28]。(a)~(d)探测结果；(e)~(h)相应的模拟结果
Fig. 6 Terahertz signals vary with time delay and phase difference when the bandwidth is 2, 3, 6, and 18 THz, respectively^[28]. (a)~(d) Recorded results; (e)~(h) corresponding simulation results

3.2 与空气探测的比较

与空气探测^[33-36]相比，水探测需要更低的探测激光能量就能产生相同水平的 TISH。对于频带为 18 THz、场强为 1 MV/cm 的太赫兹波，水膜在 5 μJ 探测光激发

下的测量结果如图 8(a)所示^[28]。空气探测时，探测光的能量必须提高到 75 μJ，才能得到同一信噪比水平的信号。图 8(b)表明在空气中探测时需要将探测光能量提高 1~2 个数量级才能达到相同的 TISH 能量。因

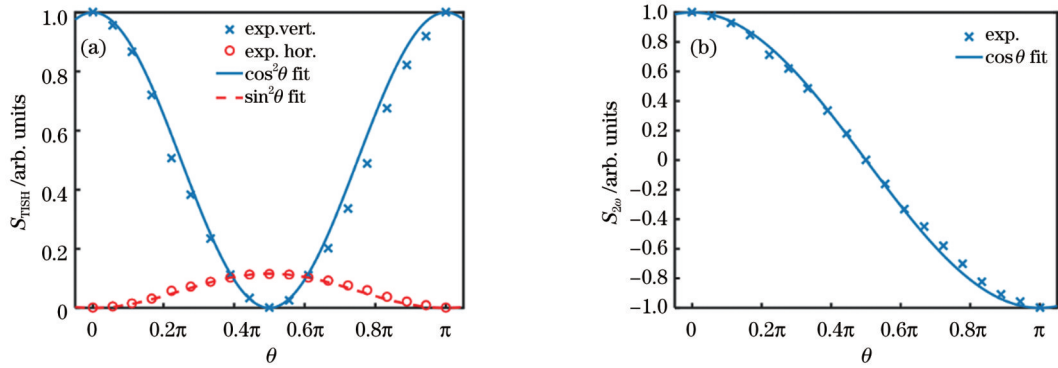


图 7 TISH 能量与探测光和太赫兹电场之间相对偏振角的关系^[29]。(a)无 CSH 时 TISH 能量与相对偏振角的关系,其中交叉和圆圈分别对应垂直和水平分量;(b)有 CSH 时 TISH 能量与相对偏振角的关系
Fig. 7 TISH energy as a function of the relative polarization angle between the probe laser and terahertz fields^[29]. (a) TISH energy as a function of the relative polarization angle in the absence of CSH, where the crosses and circles correspond to the vertical and horizontal components, respectively; (b) TISH energy as a function of the relative polarization angle in the case of CSH

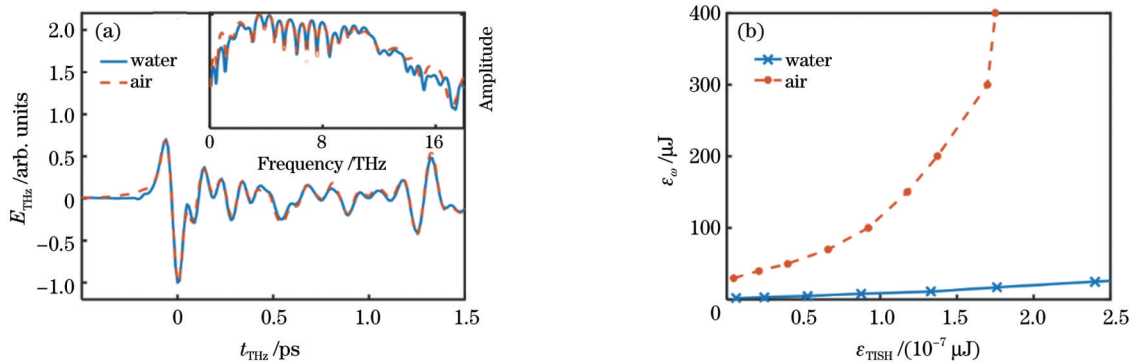


图 8 液态水探测和空气探测的比较^[29]。(a)太赫兹时域波形和相应的频谱;(b)在给定的 1 MV/cm 太赫兹电场下,产生 TISH 能量所需的探测光束的能量
Fig. 8 Comparison of the water- and air-based detection methods^[29]. (a) Terahertz time-domain waveforms and the corresponding spectra; (b) required probe beam energy to generate the TISH energy for the given terahertz field of 1 MV/cm

此,在相同的实验条件下,液态水探测的灵敏度比空气探测高 1~2 个量级。

3.3 基于液态水和空气探测的 TISH 能量比较

图 9 给出了 TISH 能量对空气和水中探测激光能量的依赖性^[28]。为清晰显示,将太赫兹场强为 0.3 MV/cm 和 1 MV/cm 时的 TISH 能量分别放大了

100 倍和 10 倍。在相同的聚焦条件下,当探测光能量分别为 35 μJ 和 2 μJ 时在空气和水中分别激发出等离子体。在同样的实验条件下,水中的探测光能量降低 1~2 个数量级就能达到与空气中探测时相同的 TISH 能量。例如,若要在 3 MV/cm 太赫兹场强下产生 $1 \times 10^{-6} \mu\text{J}$ 的 TISH 能量,在水中探测时需要 10 μJ

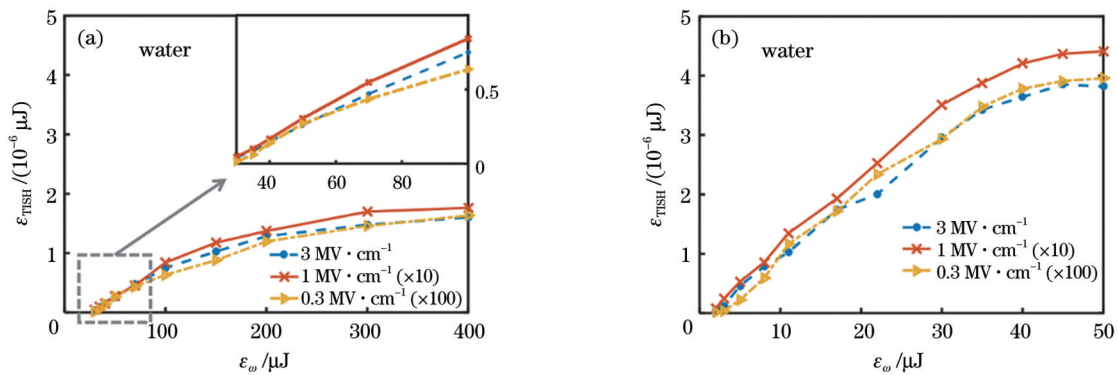


图 9 太赫兹电场强度为 0.3、1、3 MV/cm 时,TISH 能量与探测光能量的关系^[28]。(a)空气探测;(b)液态水探测
Fig. 9 Dependence of TISH energy on probe laser energy when THz field intensity is 0.3, 1, and 3 MV/cm, respectively^[28]. (a) Air-based detection method; (b) water-based detection method

的探测光,而在空气中只需要 150 μJ 的探测光。

4 基于盐溶液的宽带太赫兹脉冲相干探测

盐溶液^[37-38]的三阶非线性系数较高,因此,基于盐溶液探测的灵敏度可以显著提高,该方案为揭示液体在太赫兹范围内的三阶非线性系数和折射率提供了途径。不同盐溶液的理化性质^[39-42]差异显著,研究人员利用太赫兹光谱^[43-44]、超快红外光谱^[45-46]和太赫兹克尔效应光谱研究了其在太赫兹波段的性质^[47-49]。2022年,张明浩等^[50]证明了基于液态水的探测方法可以拓展到盐溶液。

4.1 盐溶液提高探测灵敏度

图 10(a) 显示了碘化物(碘化铯、碘化锂、碘化钠

和碘化钾)水溶液中探测的太赫兹脉冲时域波形,所有实验均在相同的条件下进行^[50]。碘化铯溶液中太赫兹信号的振幅最大,之后依次为碘化锂溶液、碘化钠溶液、碘化钾溶液和水。信号的增强归因于盐离子的加入。除碘化铯外,所有盐溶液的浓度均为 4 mol/L(碘化铯在浓度为 2 mol/L 时达到饱和)。其中,碘化铯溶液中的探测灵敏度相比其他单重盐溶液提高了 2.3 倍。虽然碘化铯溶液的浓度最低,但探测灵敏度的提高最显著。图 10(a)~(c) 显示,在相同的浓度下,碘化物水溶液中的探测灵敏度高于溴化物水溶液和氯化物水溶液,其中铯离子溶液中的探测灵敏度最高。溴化物和氯化物溶液中的探测结果如图 10(b) 和图 10(c) 所示,溴化铯因毒性和成本均较高,未纳入实验。

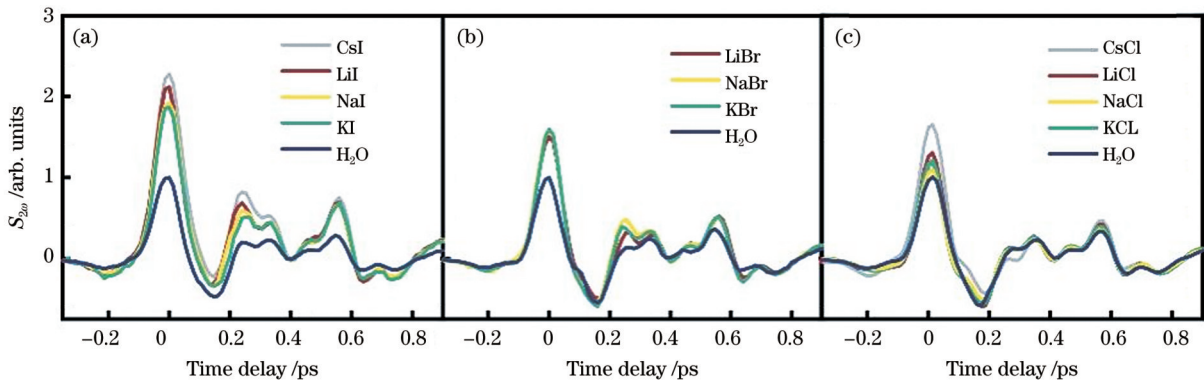


图 10 盐溶液中太赫兹电场的相干探测^[50]。(a)碘化物(碘化锂、碘化钠、碘化钾、碘化铯)水溶液;(b)溴化物(溴化锂、溴化钠、溴化钾)水溶液;(c)氯化物(氯化锂、氯化钠、氯化钾、氯化铯)水溶液

Fig. 10 Terahertz coherence detection in saline solutions^[50]. (a) Iodide aqueous solutions (LiI, NaI, KI, and CsI); (b) bromide aqueous solutions (LiBr, NaBr, and KBr); (c) chloride aqueous solutions (LiCl, NaCl, KCl, and CsCl)

盐溶液的折射率与其溶质的折射率、溶液浓度成正比,如图 11(a) 所示^[50],图中数据使用的是盐溶液在

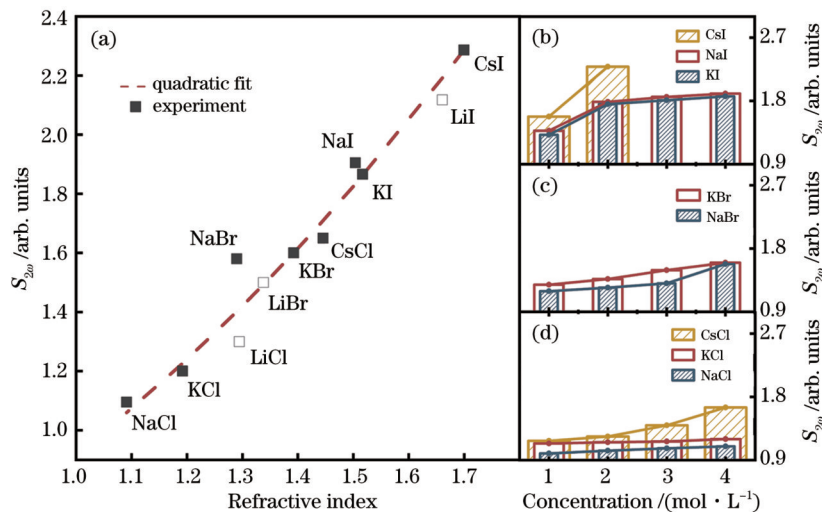


图 11 探测信号强度随溶液折射率和浓度的变化^[50]。(a)探测信号强度随溶液折射率的变化,其中虚线表示二次拟合曲线;(b)探测信号强度随碘化盐溶液浓度的变化;(c)探测信号强度随溴化盐溶液浓度的变化;(d)探测信号强度随氯化盐溶液浓度的变化

Fig. 11 Detection signal intensity varies with solution refractive index and concentration^[50]. (a) Detection signal intensity as a function of solution refractive index, where the dashed line represents the quadratic fitting curve; (b) detection signal intensity as a function of the aqueous iodide solution concentration; (c) detection signal intensity as a function of the aqueous bromide solution concentration; (d) detection signal intensity as a function of the aqueous chloride solution concentration

9 THz 下的折射率。可以发现,探测信号强度随溶液折射率的增大而单调增加,且呈二次关系。图 11(b)~(d)表明,相干探测信号强度随溶液浓度的增加而增大,信号强度的斜率也随溶液浓度发生变化。折射率较高的盐溶液具有较高的信号振幅,因此,可将检测灵敏度的提高归因于高浓度溶液折射率的增大。需要注意的是,对于碘化钠和碘化溶液,当其浓度较低时,信

号振幅的线性增大速度保持不变;然而,随着溶液浓度逐渐接近饱和,信号振幅增大的速度减慢。

4.2 相干探测信号的强度规律

图 12(a)~(c)显示了碘化盐、溴化盐和氯化盐溶液中测量的 TISH 信号^[50]。图 12(d)和图 12(e)显示信号强度随着溶液浓度的增加而增大,对比信号强度的斜率可以发现非相干信号的变化速度更快。

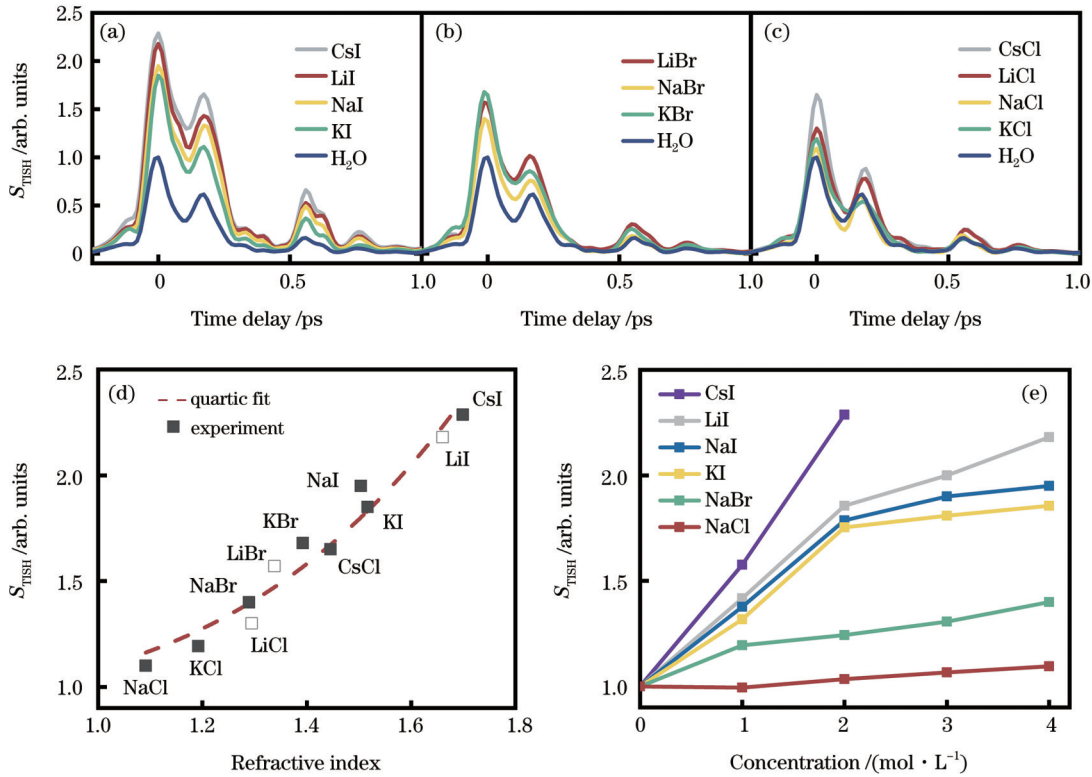


图 12 使用不同盐溶液的不相干检测^[50]。(a)在碘化盐(碘化锂、碘化钠、碘化钾、碘化铯)溶液和纯水中探测的 TISH 信号的比较; (b)在溴化盐(溴化锂、溴化钠、溴化钾)溶液和纯水中探测的 TISH 信号的比较; (c)在氯化盐(氯化锂、氯化钠、氯化钾、氯化铯)溶液和纯水中探测的 TISH 信号的比较; (d) TISH 能量与不同溶液折射率的关系曲线; (e) TISH 能量与溶液浓度的依赖关系

Fig. 12 Incoherent detection using different aqueous salt solutions^[50]. (a) Comparison of TISH signal detected in aqueous iodide (LiI, NaI, KI, and CsI) solutions and pure water; (b) comparison of TISH signal detected in aqueous bromide (LiBr, NaBr, and KBr) solutions and pure water; (c) comparison TISH signal detected in aqueous chloride (LiCl, NaCl, KCl, and CsCl) solutions and pure water; (d) measured TISH energy as a function of the refractive index of different solutions; (e) the dependence of measured TISH energy on the solution concentration

4.3 相干探测的太赫兹时域波形比较

在不同盐溶液中相干探测得到的归一化太赫兹时域波形如图 13(a)~(c)所示^[50]。与在纯水中相干探测得到的归一化太赫兹时域波形相比,在不同盐溶液中相干探测得到的归一化太赫兹时域波形的前半周期保持相同的形状,而后半周期的波形有所减弱,且衰减量与各盐溶液的折射率成正相关,如图 13(d)所示。实验中的 TISH 是在液体等离子体形成时产生的,探测激光激发的电离主要发生在太赫兹脉冲的前半部分,太赫兹脉冲和形成的等离子体主要在太赫兹脉冲的后半部分相互作用,被等离子体吸收的太赫兹时域波形的后半部分衰减显著。此外,在具有较高折射率的盐溶液中,激光会形

成较强的等离子体丝,从而会导致更大的太赫兹电场衰减。

5 基于乙醇的太赫兹脉冲的相干探测

尽管基于液态水产生太赫兹波并进行相干探测^[51-52]具有很大的潜力,但水对太赫兹波的响应要弱于对其他液体(如乙醇^[53])的响应。乙醇的电离能比水低^[54-55],因此,它比水更容易电离,在较低的探测激光能量下就能形成液体等离子体。此外,乙醇的三阶非线性系数较水的大^[56-57],因此,乙醇在太赫兹液体光子学中的应用更具潜力。已有研究证明乙醇在太赫兹波段^[58]比纯水具有更高的分子响应。此外,相关研究已经证实,乙醇比纯水能发出

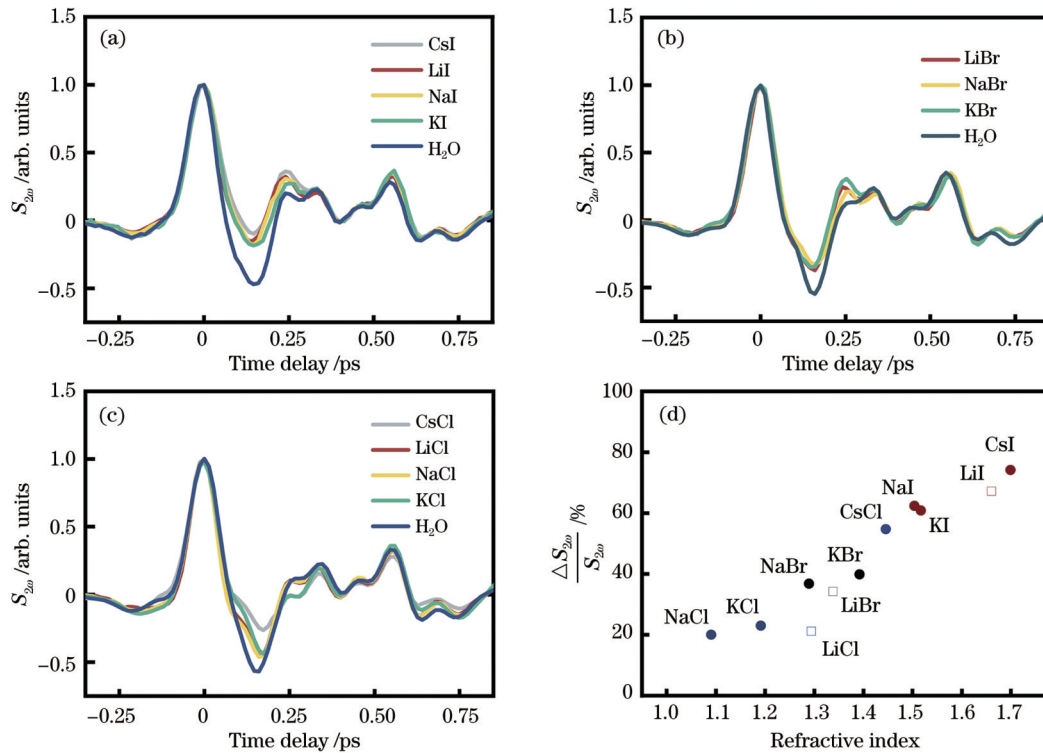


图 13 在不同溶液中探测的归一化太赫兹时域波形以及盐溶液与纯水相比振幅在第二半周期的差异^[50]。(a)在碘化盐(碘化锂、碘化钠、碘化钾、碘化铯)溶液中探测的归一化太赫兹时域波形;(b)在溴化盐(溴化锂、溴化钠、溴化钾)溶液中探测的归一化太赫兹时域波形;(c)在氯化盐(氯化锂、氯化钠、氯化钾、氯化铯)溶液中探测的归一化太赫兹时域波形;(d)盐溶液与纯水相比振幅在第二半周期的差异随盐溶液折射率的变化

Fig. 13 Normalized terahertz time-domain waveforms detected in different solutions and differences of the amplitude in the second half-cycle between aqueous salt solutions and pure water^[50]. (a) Normalized terahertz time-domain waveforms detected in aqueous iodide (LiI, NaI, KI, and CsI) solutions; (b) normalized terahertz time-domain waveforms detected in aqueous bromide (LiBr, NaBr, and KBr) solutions; (c) normalized terahertz time-domain waveforms detected in aqueous chloride (LiCl, NaCl, KCl, and CsCl) solutions; (d) differences of the amplitude in the second half-cycle between aqueous salt solutions and pure water versus refractive index of saline solutions

更强的太赫兹波。2022年,本课题组成员肖文等基于乙醇对太赫兹脉冲进行了相干探测,结果显示,乙醇是一种有效的太赫兹波相干探测介质,与纯水相比,乙醇相干探测的灵敏度和信噪比进一步提高。

5.1 基于乙醇、水和空气测量的信号比较

实验中,太赫兹波峰值场强为 4.6 MV/cm,探测光能量设置为 15 μJ。BBO 晶体的最大 SH 转换效率

约为 5%,因此,CSH 光的最大能量约为 0.75 μJ。在这种情况下,虽然 CSH 的偏振可能不平行于太赫兹电场,无法确保 CSH 和 TISH 完全相干,但可以通过在 BBO 晶体后插入一个 400 nm 的半波片来改变偏振方向,满足相干探测要求。在相同的太赫兹电场强度和探测光能量下,基于乙醇、水和空气探测到的太赫兹时域波形如图 14(a)所示^[27],基于乙醇探测的信号

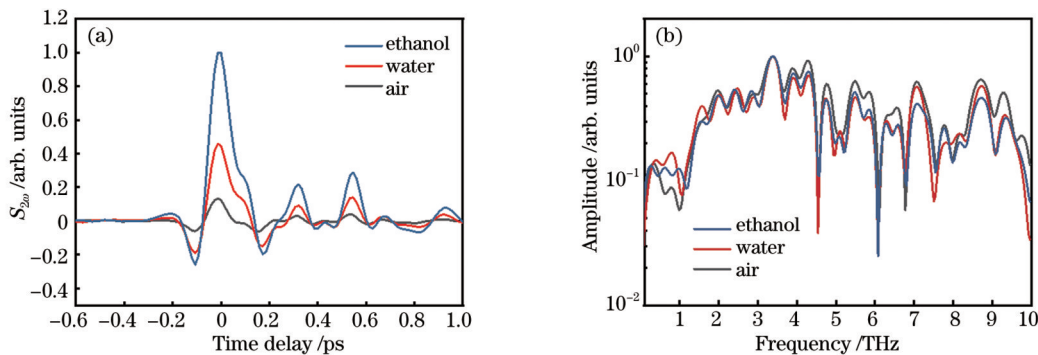


图 14 液体膜对太赫兹波的相干检测^[27]。(a)通过乙醇、纯水和空气检测到的太赫兹波形;(b)对应的频谱

Fig. 14 Coherent detection of terahertz wave by liquid film^[27]. (a) Terahertz waveforms detected by ethanol, pure water, and air; (b) the corresponding frequency spectra

振幅最大,基于水探测的信号振幅次之,基于空气探测的信号振幅最小。由图 14(b)可以看出,基于三种不同液体测量的太赫兹频谱较吻合。

将探测光能量固定在 $15 \mu\text{J}$,不同太赫兹电场下的测量结果如图 15(a)所示^[27],拟合线为乙醇和纯水中探测到的太赫兹波峰值。拟合线的斜率表明,乙醇

在太赫兹波段的灵敏度高于水。图 15(b)给出了乙醇和纯水在 $5\sim 30 \mu\text{J}$ 探测光能量下的相干探测信号。乙醇在任何探测光下都比纯水具有更高的响应,即使探测光能量低至 $5 \mu\text{J}$,乙醇的时域波形仍具有良好的信噪比,为低激光能量的太赫兹相干探测提供了新途径。

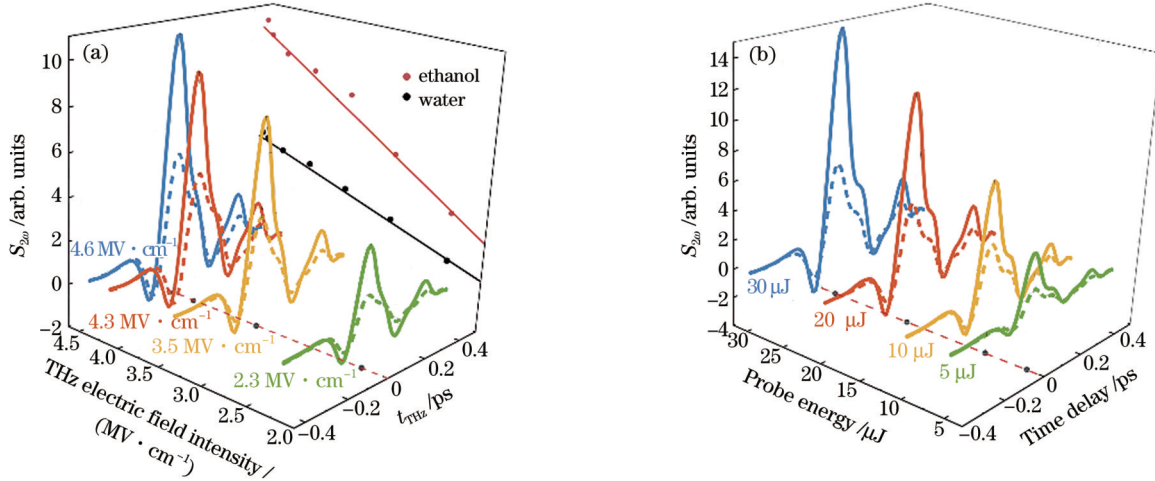


图 15 基于液膜的太赫兹相干检测^[27]。(a)在不同太赫兹电场强度下基于乙醇(实线)和水(虚线)测量的太赫兹时域波形,线性拟合结果是乙醇和水探测信号的峰值;(b)在 $5\sim 30 \mu\text{J}$ 探测光能量下基于乙醇(实线)和纯水(虚线)探测的波形

Fig. 15 Terahertz coherent detection based on liquid film^[27]. (a) Terahertz time-domain waveforms detected by ethanol (solid lines) and water (dotted lines) at different terahertz electric field intensities, and the linear fitting results represent the ethanol and water detection signal peaks; (b) waveforms detected by ethanol (solid lines) and pure water (dotted lines) under probe laser energy from $5 \mu\text{J}$ to $30 \mu\text{J}$

5.2 CSH 光束偏振敏感探测

为进一步研究 CSH 的偏振方向对相干探测的影响,建立 x 轴沿水平方向、 y 轴沿竖直方向的空间直角坐标系,太赫兹场垂直偏振, TISH 平行于 y 轴, $E_{\text{TISH}}^y = \chi_{\text{yyy}}^{(3)} (E_{\omega}^y)^2 E_{\text{THz}}^y$ 。定义 α 为 BBO 晶体的 \hat{e} 轴与水平方向(x 轴)的夹角,旋转角度 α 引起的基波偏振方向的轻微变化忽略不计。旋转 BBO 方位角所记录的时域波形如图 16 所示^[27]。如灰色虚线所示,CSH 强度在 $\alpha = 0^\circ(180^\circ)$ 时最大^[59],在 $\alpha = 90^\circ(270^\circ)$ 时最小。由于 CSH 的偏振方向总是沿着 BBO 晶体的 \hat{e} 轴,所以 CSH 在 $\alpha = 0^\circ(180^\circ)$ 时是水平偏振的。在这种情况下,CSH 和 TISH 电场相互垂直无法发生干涉,导致非相干探测。理论上,当 $\alpha = 90^\circ(270^\circ)$ 时,CSH 强度应该是零,然而,在实验中,仍然获得了一个可检测到的 CSH 信号,如图 16 中的黑色点线所示,这可能是由探测光在 BBO 晶体上的入射方向轻微偏离正入射导致的。测量到的与 TISH 平行的垂直偏振 CSH 光的能量为微焦量级,满足相干探测要求。其他角度,比如 $\alpha = 45^\circ(225^\circ)$,可使式(2)中的第一项和第三项具有可比性,实现混合探测。

5.3 使用乙醇-水混合溶液进行太赫兹脉冲的相干探测

在纯水和乙醇测量结果和理论分析的基础上,研

究人员进一步用不同浓度的乙醇-水混合溶液来探测太赫兹脉冲,结果如图 17(a)中的实线所示^[27],探测信号的振幅随乙醇体积分数的增加而增大。

$$\Delta S_{2\omega}(t_{\text{THz}}) = a_i S_{2\omega}^{\text{water}}(t_{\text{THz}}) + b_i S_{2\omega}^{\text{ethanol}}(t_{\text{THz}}), \quad (7)$$

式中: $S_{2\omega}^{\text{water}}(t_{\text{THz}})$ 和 $S_{2\omega}^{\text{ethanol}}(t_{\text{THz}})$ 分别表示在纯水和乙醇中测量的相干探测信号的振幅,用式(7)计算得到的混合溶液的拟合结果如图 17(a)中的虚线所示; a_i 和 b_i 分别为水和乙醇的比例系数,与乙醇的体积分数有关。由图 17(a)可知模拟结果与实测结果吻合较好,表明混合溶液的相干探测可以分解为纯水和纯乙醇的相干探测信号的线性叠加。显然,乙醇和水对相干探测的贡献取决于亚皮秒时间尺度上乙醇和水的分子数量,揭示了混合物中分子间振动模式的独立性。以往的低频拉曼光谱研究表明乙醇-水混合物中乙醇与水的相互作用是可以忽略的,因此乙醇和水分子之间的相互作用是弱的^[60]。在分子水平上,混合溶液不是处于理想的混合态,而是处于“微相分离”的状态,大部分的水-乙醇键可能在分子振荡期间被解离。值得注意的是,当时间尺度超过几皮秒后,线性叠加结果与测量数据出现了偏差。这是因为,在不同浓度下,不同的分子弛豫模式占主导地位,太赫兹克尔效应^[58]研究揭示了这一点。混合溶液中分子的相互作用比较复杂,需要进行更深入的实验来进一步研究。

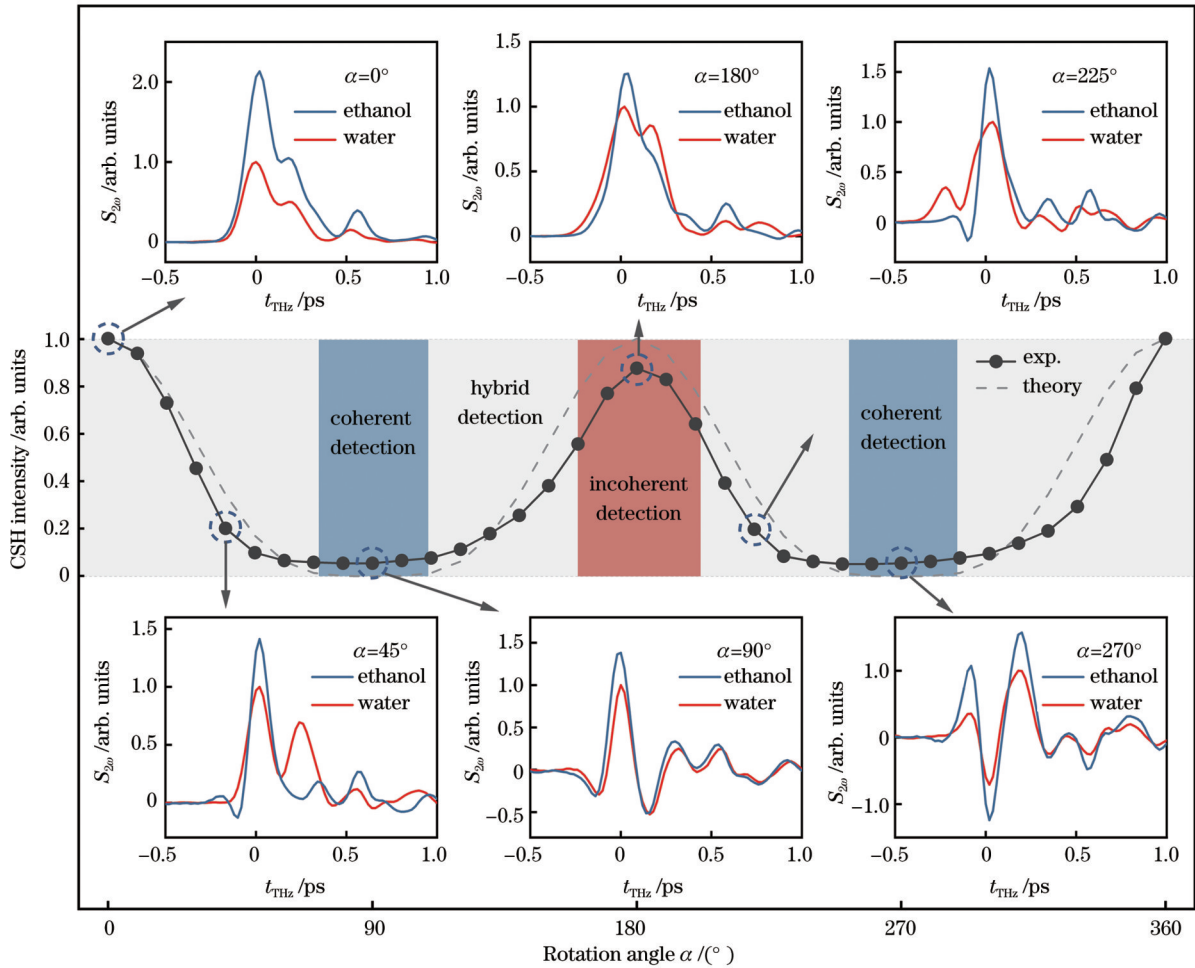


图 16 不同 BBO 角度下探测的太赫兹波形^[27]。当 $\alpha = 0^\circ(180^\circ)$ 时, CSH 垂直于 TISH, 非相干探测; 当 $\alpha = 90^\circ(270^\circ)$ 时, CSH 与 TISH 平行, 相干探测; 当 $\alpha = 45^\circ(225^\circ)$ 时, 混合探测。黑点和灰色虚线是测量和理论的 CSH 能量值
 Fig. 16 Measured waveforms at different BBO angle values^[27]. When $\alpha = 0^\circ(180^\circ)$, CSH is perpendicular polarized to TISH, leads to incoherent detection. When $\alpha = 90^\circ(270^\circ)$, the polarizations of CSH and TISH are parallel, which presents as coherent detection. When $\alpha = 45^\circ(225^\circ)$, a hybrid detection is introduced. The black dots and gray dashed line are the measured and theoretical CSH energy, respectively

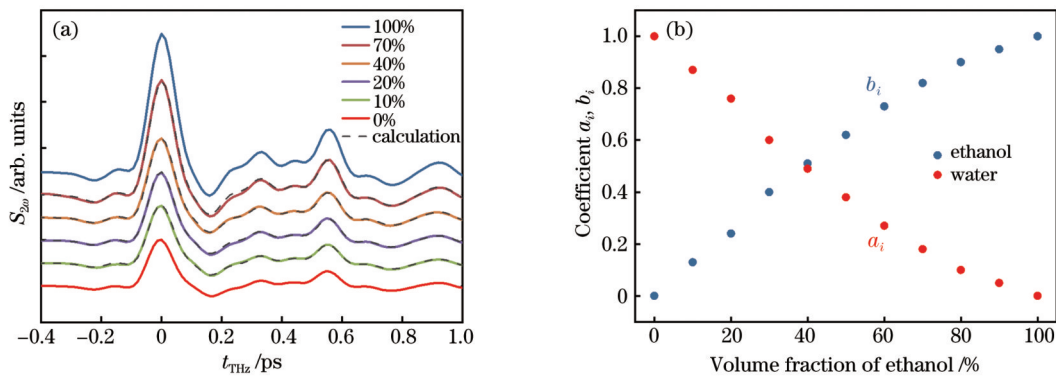


图 17 用乙醇-水混合溶液进行相干探测^[27]。(a) 相干探测的太赫兹时域波形和拟合结果; (b) 水和乙醇的系数
 Fig. 17 Coherent detection using ethanol-water mixture^[27]. (a) Measured terahertz time-domain waveforms and fitting result of coherent detection by ethanol-water mixtures; (b) coefficients of water and ethanol

6 结束语

本文主要综述了基于不同种类液体探测太赫兹波的特性。相比于空气探测方法, 液体探测方法所需的

探测激光能量低至几微焦。在相同的探测条件下, 液体探测方法的灵敏度比空气高一个数量级。与普通的固体探测技术相比, 液体探测具有更大的探测带宽。与纯水探测相比, 盐溶液探测的灵敏度更高, 而且随着

盐溶液浓度增大,探测的太赫兹信号强度更大。此外,乙醇-水混合溶液的太赫兹脉冲相干探测结果显示:随着混合物中乙醇所占比例的增加,探测的太赫兹信号强度增大。另外,糖溶液以及丙酮等有机溶剂也具有较高的三阶非线性系数,能增大探测灵敏度,可以基于此进行相应的研究。液体探测太赫兹波相对于气体和固体探测来说具有独特优势,为相干探测宽带太赫兹脉冲提供了一个新视角,在太赫兹时域光谱和太赫兹遥感方面具有巨大的应用潜力。

参 考 文 献

- [1] 蒋广通, 张亮亮, 吴同, 等. 离轴涡旋光束诱导空气等离子体产生太赫兹波[J]. 中国激光, 2019, 46(6): 0614026.
Jiang G T, Zhang L L, Wu T, et al. THz wave generation from air plasma induced by off-axis vortex beam[J]. Chinese Journal of Lasers, 2019, 46(6): 0614026.
- [2] 戴建明, 张伟帆, 陈宇轩, 等. 液态水辐射源产生太赫兹波的研究进展[J]. 中国激光, 2021, 48(19): 1914001.
Dai J M, Zhang Y F, Chen Y X, et al. Research progress on terahertz wave generation from liquid water[J]. Chinese Journal of Lasers, 2021, 48(19): 1914001.
- [3] 徐强, 苏强, 鲁丹, 等. 基于激光成丝的太赫兹时域光谱系统研究综述[J]. 中国激光, 2019, 46(6): 0614010.
Xu Q, Su Q, Lu D, et al. Review of terahertz time-domain spectroscopy systems based on laser filament[J]. Chinese Journal of Lasers, 2019, 46(6): 0614010.
- [4] Zhou R Y, Wang C, Xu W D, et al. Biological applications of terahertz technology based on nanomaterials and nanostructures[J]. Nanoscale, 2019, 11(8): 3445-3457.
- [5] Saavedra G, Tan M M, Elson D J, et al. Experimental analysis of nonlinear impairments in fibre optic transmission systems up to 7.3 THz[J]. Journal of Lightwave Technology, 2017, 35(21): 4809-4816.
- [6] 冀宝庆, 李香宇, 王艳红, 等. 近红外与太赫兹双波段局域场增强结构设计[J]. 激光与光电子学进展, 2023, 60(5): 0530004.
Ji B Q, Li X Y, Wang Y H, et al. Structure design of near-infrared and terahertz dual-band local field enhancement[J]. Laser & Optoelectronics Progress, 2023, 60(5): 0530004.
- [7] Dash J, Ray S, Devi N, et al. Fine-tuning of terahertz resonances in hydrogen-bonded organic molecular complexes[J]. Journal of Molecular Structure, 2019, 1184: 495-502.
- [8] 张泽亮, 齐鹏飞, 郭兰军, 等. 太赫兹超分辨近场成像方法研究综述[J]. 光学学报, 2023, 43(6): 0600001.
Zhang Z L, Qi P F, Guo L J, et al. Review on super-resolution near-field terahertz imaging methods[J]. Acta Optica Sinica, 2023, 43(6): 0600001.
- [9] Kemp M C, Taday P F, Cole B E, et al. Security applications of terahertz technology[J]. Proceedings of SPIE, 2003, 5070: 44-52.
- [10] van Exter M, Fattinger C, Grischkowsky D. Terahertz time-domain spectroscopy of water vapor[J]. Optics Letters, 1989, 14(20): 1128-1130.
- [11] Zaytsev K I, Dolganova I N, Chernomyrdin N V, et al. The progress and perspectives of terahertz technology for diagnosis of neoplasms: a review[J]. Journal of Optics, 2020, 22(1): 013001.
- [12] Hirata J, Kurokawa N, Okano M, et al. Evaluation of crystallinity and hydrogen bond formation in stereo complex poly (lactic acid) films by terahertz time-domain spectroscopy[J]. Macromolecules, 2020, 53(16): 7171-7177.
- [13] Hoshina H, Saito Y, Furuhashi T, et al. Terahertz spectroscopy for characterization of hydrogen bonding and cross-linked structure dynamics in polyurethane[J]. Journal of Infrared, Millimeter, and Terahertz Waves, 2020, 41(3): 265-275.
- [14] Williams B S, Kumar S, Callebaut H, et al. Terahertz quantum cascade lasers using resonant-phonon depopulation and metal-metal waveguides[J]. Proceedings of SPIE, 2004, 5365: 194-202.
- [15] Williams B S, Callebaut H, Kumar S, et al. 3.4-THz quantum cascade laser based on longitudinal-optical-phonon scattering for depopulation[J]. Applied Physics Letters, 2003, 82(7): 1015-1017.
- [16] Sun Y W, Sy M Y, Wang Y X J, et al. A promising diagnostic method: terahertz pulsed imaging and spectroscopy[J]. World Journal of Radiology, 2011, 3(3): 55-65.
- [17] Xiong H, Wu Q A, Lu Y, et al. Polarization-resolved edge states in terahertz topological photonic crystal[J]. Optics Express, 2019, 27(16): 22819-22826.
- [18] Nagel M, Richter F, Haring-Bolivar P, et al. A functionalized THz sensor for marker-free DNA analysis[J]. Physics in Medicine and Biology, 2003, 48(22): 3625-3636.
- [19] Xu K Y, Liu M K, Arbab M H. Broadband terahertz time-domain polarimetry based on air plasma filament emissions and spinning electro-optic sampling in GaP[J]. Applied Physics Letters, 2022, 120(18): 181107.
- [20] Nahata A, Auston D H, Heinz T F, et al. Coherent detection of freely propagating terahertz radiation by electro-optic sampling[J]. Applied Physics Letters, 1996, 68(2): 150-152.
- [21] Wu Q, Zhang X C. Free-space electro-optic sampling of terahertz beams[J]. Applied Physics Letters, 1995, 67(24): 3523-3525.
- [22] Lu X F, Karpowicz N, Chen Y Q, et al. Systematic study of broadband terahertz gas sensor[J]. Applied Physics Letters, 2008, 93(26): 261106.
- [23] Dai J M, Xie X, Zhang X C. Detection of broadband terahertz waves with a laser-induced plasma in gases[J]. Physical Review Letters, 2006, 97(10): 103903.
- [24] Dey I, Jana K, Fedorov V Y, et al. Highly efficient broadband terahertz generation from ultrashort laser filamentation in liquids[J]. Nature Communications, 2017, 8: 1184.
- [25] Jin Q, Williams K, Yiwen E, et al. Observation of broadband terahertz wave generation from liquid water[J]. Applied Physics Letters, 2017, 111(7): 071103.
- [26] Minardi S, Gopal A, Tatarakis M, et al. Time-resolved refractive index and absorption mapping of light-plasma filaments in water[J]. Optics Letters, 2007, 33(1): 86-88.
- [27] Xiao W, Zhang M H, Zhang R, et al. Efficient coherent detection of terahertz pulses based on ethanol[J]. Applied Physics Letters, 2023, 122(6): 061105.
- [28] 谭永. 水等离子体太赫兹波谱特性的测量与研究[D]. 北京: 北京理工大学, 2021.
Tan Y. Measurement and study on the terahertz spectrum characteristics of plasma in liquid water[D]. Beijing Institute of Technology, 2021.
- [29] Tan Y, Zhao H, Wang W M, et al. Water-based coherent detection of broadband terahertz pulses[J]. Physical Review Letters, 2022, 128(9): 093902.
- [30] Leitenstorfer A, Hunsche S, Shah J, et al. Detectors and sources for ultrabroadband electro-optic sampling: experiment and theory [J]. Applied Physics Letters, 1999, 74(11): 1516-1518.
- [31] Casalbuoni S, Schlarb H, Schmidt B, et al. Numerical studies on the electro-optic detection of femtosecond electron bunches[J]. Physical Review Special Topics, 2008, 11(7): 072802.
- [32] Zhao H, Tan Y, Zhang L L, et al. Ultrafast hydrogen bond dynamics of liquid water revealed by terahertz-induced transient birefringence[J]. Light: Science & Applications, 2020, 9: 136.
- [33] Woerner M, Reimann K. Harnessing terahertz polarization[J]. Nature Photonics, 2009, 3(9): 495-496.
- [34] Liu J L, Dai J M, Chin S L, et al. Broadband terahertz wave remote sensing using coherent manipulation of fluorescence from asymmetrically ionized gases[J]. Nature Photonics, 2010, 4(9): 627-631.
- [35] Karpowicz N, Dai J M, Lu X F, et al. Coherent heterodyne time-domain spectrometry covering the entire "terahertz gap" [J]. Applied Physics Letters, 2008, 92(1): 011131.

- [36] Li C Y, Seletskiy D V, Yang Z, et al. Broadband field-resolved terahertz detection via laser induced air plasma with controlled optical bias[J]. *Optics Express*, 2015, 23(9): 11436-11443.
- [37] Débarre D, Beaurepaire E. Quantitative characterization of biological liquids for third-harmonic generation microscopy[J]. *Biophysical Journal*, 2007, 92(2): 603-612.
- [38] Kucia W E, Sharma G, Joseph C S, et al. Optical Kerr effect of tRNA solution induced by femtosecond laser pulses[J]. *Chemical Physics Letters*, 2016, 662: 132-136.
- [39] Kaminsky M. Ion-solvent interaction and the viscosity of strong-electrolyte solutions[J]. *Discussions of the Faraday Society*, 1957, 24: 171-179.
- [40] McAllister R A. The viscosity of liquid mixtures[J]. *AIChE Journal*, 1960, 6(3): 427-431.
- [41] Lazzús J A. A group contribution method to predict the melting point of ionic liquids[J]. *Fluid Phase Equilibria*, 2012, 313: 1-6.
- [42] Ryckaert J P, Bellemans A. Molecular dynamics of liquid *n*-butane near its boiling point[J]. *Chemical Physics Letters*, 1975, 30(1): 123-125.
- [43] Funkner S, Niehues G, Schmidt D A, et al. Watching the low-frequency motions in aqueous salt solutions: the terahertz vibrational signatures of hydrated ions[J]. *Journal of the American Chemical Society*, 2012, 134(2): 1030-1035.
- [44] Sebastiani F, Wolf S L P, Born B, et al. Water dynamics from THz spectroscopy reveal the locus of a liquid-liquid binodal limit in aqueous CaCO₃ solutions[J]. *Angewandte Chemie International Edition*, 2017, 56(2): 490-495.
- [45] Ohtaki H, Radnai T. Structure and dynamics of hydrated ions[J]. *Chemical Reviews*, 1993, 93(3): 1157-1204.
- [46] Dodo T, Sugawa M, Nonaka E, et al. Absorption of far-infrared radiation by alkali halide aqueous solutions[J]. *The Journal of Chemical Physics*, 1995, 102(15): 6208-6211.
- [47] Freys E, Degert J. Terahertz Kerr effect[J]. *Nature Photonics*, 2010, 4(3): 131-132.
- [48] Zhao H, Tan Y, Zhang R, et al. Anion-water hydrogen bond vibration revealed by the terahertz Kerr effect[J]. *Optics Letters*, 2021, 46(2): 230-233.
- [49] Tan Y, Zhao H, Zhang R, et al. Ultrafast optical pulse polarization modulation based on the terahertz-induced Kerr effect in low-density polyethylene[J]. *Optics Express*, 2020, 28(23): 35330-35338.
- [50] Zhang M H, Xiao W, Wang W M, et al. Highly sensitive detection of broadband terahertz waves using aqueous salt solutions[J]. *Optics Express*, 2022, 30(21): 39142-39151.
- [51] Yiwen E, Jin Q, Tcytkin A, et al. Terahertz wave generation from liquid water films via laser-induced breakdown[J]. *Applied Physics Letters*, 2018, 113(18): 181103.
- [52] Zhang L L, Wang W M, Wu T, et al. Strong terahertz radiation from a liquid-water line[J]. *Physical Review Applied*, 2019, 12(1): 014005.
- [53] Zalden P, Song L W, Wu X J, et al. Molecular polarizability anisotropy of liquid water revealed by terahertz-induced transient orientation[J]. *Nature Communications*, 2018, 9: 2142.
- [54] Watanabe K, Nakayama T, Mottl J. Ionization potentials of some molecules[J]. *Journal of Quantitative Spectroscopy and Radiative Transfer*, 1962, 2(4): 369-382.
- [55] Beckey H D, Levsen K, Röllgen F W, et al. Field ionization mass spectrometry of organic compounds[J]. *Surface Science*, 1978, 70(1): 325-362.
- [56] Gaiduk A P, Pham T A, Govoni M, et al. Electron affinity of liquid water[J]. *Nature Communications*, 2018, 9: 247.
- [57] Noack J, Vogel A. Laser-induced plasma formation in water at nanosecond to femtosecond time scales: calculation of thresholds, absorption coefficients, and energy density[J]. *IEEE Journal of Quantum Electronics*, 1999, 35(8): 1156-1167.
- [58] Zhao H, Tan Y, Zhang R, et al. Molecular dynamic investigation of ethanol-water mixture by terahertz-induced Kerr effect[J]. *Optics Express*, 2021, 29(22): 36379-36388.
- [59] Kress M, Löffler T, Eden S, et al. Terahertz-pulse generation by photoionization of air with laser pulses composed of both fundamental and second-harmonic waves[J]. *Optics Letters*, 2004, 29(10): 1120-1122.
- [60] Egashira K, Nishi N. Low-frequency Raman spectroscopy of ethanol-water binary solution: evidence for self-association of solute and solvent molecules[J]. *The Journal of Physical Chemistry B*, 1998, 102(21): 4054-4057.

High-Sensitivity Detection of Terahertz Pulse Based on Liquids

Wang Guoyang¹, Zhang Minghao¹, Xiao Wen¹, Zhang Cunlin¹, Wang Weimin¹, Zhang Liangliang²

¹Key Laboratory of Terahertz Optoelectronics (MOE), Department of Physics, Capital Normal University, Beijing 100048, China;

²Department of Physics, Renmin University of China, Beijing 100872, China

Abstract

Significance Terahertz (THz) waves are electromagnetic waves with frequencies ranging from 0.1 to 10 THz, between microwave and infrared. With the development of femtosecond lasers, terahertz waves are gradually being widely used in imaging technology, communication technology, medical and health, biochemical technology, nondestructive testing, security inspection technology, and other fields. Currently, the energy required to generate terahertz waves is relatively low, and detection technologies with high sensitivity and bandwidth are urgently required. The most widely used techniques in the field of terahertz wave coherent detection are solid dielectric-based photoconductive sampling and electro-optic sampling. However, owing to the factors such as non-instantaneous response of dielectric carriers, phonon absorption, and the Reststrahlen frequency band, it is difficult for the detection bandwidth to cover the entire terahertz band. Gas media are not affected by these factors, and the coherent detection of sufficiently wideband terahertz waves can be achieved through air-biased and light field-biased coherent detection. However, to achieve high detection sensitivity, the femtosecond laser beam to be detected ionizes air into plasma. Owing to the high excitation threshold of plasma in air, the energy of the laser beam is usually several hundred microjoules (μJ). Solids and gases have been proven to be suitable media for detecting terahertz waves, and the potential use of liquids for the coherent detection of terahertz waves has been an important issue of interest for researchers in the terahertz field. Related research has confirmed that liquids can be used for the generation of terahertz

waves, and the intensity of such generated terahertz waves is 1.8 times greater than that of air. Compared to gases, liquids have higher molecular densities and nonlinear coefficients, which results in higher free electron concentrations and lower ionization thresholds in liquid plasmas. Compared with solids, the fluidity of liquids increases their damage threshold and allows them to self-repair.

Progress This article reviews the coherent detection of broadband terahertz pulses in pure water, salt solution, and ethanol. Water requires lower detection energy than air to generate the same level of terahertz induced second harmonic (TISH). The measurement results for a water film under $5\ \mu\text{J}$ probe light excitation for a terahertz wave with a frequency band of 18 THz and a field intensity of $1\ \text{MV}/\text{cm}$ are shown in Fig. 8. When detecting in air, the energy of the detected light must be increased to $75\ \mu\text{J}$ to obtain a signal with the same signal-to-noise ratio level. These results indicate that it is necessary to increase the detection light energy by 1–2 orders of magnitude to achieve the same TISH energy in air. Therefore, under the same experimental conditions, the sensitivity of liquid water detection is 1–2 orders of magnitude greater than that of air (Figs. 8 and 9). Because of the high third-order nonlinear coefficient of salt solutions, the signal intensity of coherent detection increases with increasing solution concentration, and the slope of the signal intensity also changes accordingly. Salts with a higher refractive index have a higher signal amplitude; therefore, the improvement in detection sensitivity is attributed to the increase in the refractive index of high-concentration solutions (Figs. 10 and 11). Ethanol has a third-order nonlinear coefficient greater than that of water, making it easier to ionize. A lower detection energy is required to form liquid plasma, and ethanol has a higher molecular response than pure water in the terahertz band. When the detection light energy is fixed at $15\ \mu\text{J}$, the sensitivity of ethanol in the terahertz band is higher than that of water. We compared the coherent detection signals of ethanol and pure water under different detection energies of $5\text{--}30\ \mu\text{J}$, and found that ethanol has a higher response than pure water under any detection light. Even if the detection energy is as low as $5\ \mu\text{J}$, the time-domain waveform of ethanol still has a good signal-to-noise ratio, providing new research prospects for low-laser-energy terahertz coherent detection (Fig. 15). The liquid-based terahertz wave coherent detection scheme expands the variety of terahertz wave detectors, providing the possibility of revealing molecular interaction mechanisms in biological liquid environments.

Conclusions and Prospects Liquid detection of terahertz waves has unique advantages over gases and solids, providing a new perspective for the coherent detection of broadband terahertz pulses, which has great potential in terahertz time-domain spectral applications and remote sensing.

Key words nonlinear optics; terahertz wave; coherent detection; liquid plasma; four-wave mixing